Balance Control of a Bikebot for Studying Human Dynamic Postural Balance Motor Control

Yizhai Zhang, Pengcheng Wang, Jingang Yi, and Dezhen Song

***Abstract*— We present the development of the gyroscopic-balanced control of an autonomous bikebot. The bikebot is an actively controlled bicycle-based robotic platform developed to study human dynamic postural balance motor skills through unstable physical human-robot interactions. We first present a dynamic model and analysis for the bikebot. A nonlinear balancing controller is designed to stabilize the underactuated bikebot on an orbital trajectory around the unstable equilibrium point that is coupled with another orbit of the actuated gyro-balancer. We demonstrate the analysis and control design with experimental validations. Finally, we present a set of human riding experiments to show how the bikebot can be used to perturb and excite human sensorimotor feedback loop for dynamic postural balance motor skills.**

I. Introduction

Human with trained motor skills can fluidly and flexibly interact with machines while smart machines can also provide motor assistance and enhancement to facilitate human's motor skills learning [1]. Many efficient human-robot interactions are unstable [2], [3]. We consider using rider-bikebot interactions as a new means to examine a sensorimotor theory for modeling and shaping postural balancing and other functional whole-body motor activities.

Bikebot is an actively controlled bicycle-based robot. The recent study in [4] demonstrates that human neuro-control has different, complementary sensitivities of balancing stability between riding the bicycle and quiet stance. Although studying physical interactions between the rider and the passive bicycle is reported in recent years [4]–[7], the bikebot provides active perturbation to break rider's sensorimotor feedback loop through actively controlled steering, velocity, and balancing. Compared to other motor skills such as quiet stance [8], riding the bikebot requires the coordinated control of multi-limb and body movements following the sensorimotor cues. Therefore, the bikebot offers a new platform for studying human postural balance motor skills through unstable physical human-robot interactions.

In this paper, we present the dynamic modeling, analysis and balance control for the bikebot system. The dynamic model of the riderless gyro-balancer bicycle is first developed. We analyze the bikebot dynamic model and present a pair of coupled oscillating orbits for the bikebot roll motion and a flywheel's pivoting motion. The balancing control design is then to regulate the bikebot motions to follow these orbital trajectories. An energy shaping method is used to design the orbital following controller. We present experiments to demonstrate the balancing analysis and control design. Finally, human riding experiments are presented to show the feasibility of using bikebot to perturb and excite human sensorimotor postural balance feedback mechanisms.

Besides the new bikebot design and demonstrating the feasibility to perturb and excite human postural balance control, additional contributions of this work are twofold. First, the presented bikebot dynamic model captures a class of underactuated robotic systems in which the coupled effects between the actuated component (gyro-balancer) and the underactuated component (bikebot roll motion) are through force/torque and energy exchange. Following the modeling analysis, we propose a coupled orbital following control design to balance the bikebot. This design complements the orbital stabilization approach in [9], [10] where virtual displacement constraints, rather than force/torque constraints, are introduced and used. Second, comparing with other related work in which autonomous motorcycles or bicycles are designed at a moving velocity [11]–[17], we have successfully demonstrated a more challenging task to balance the stationary bikebot at zero velocity. Moreover, we analytically give an estimation of the domain of attraction under the control design.

The remainder of the paper is organized as follows. We review the related work in Section II and then discuss the bikebot dynamic model in Section III. The balancing control and analysis are presented in Section IV. Experiments are presented to demonstrate the design in Section V. We finally conclude the paper and discuss the future work in Section VI.

II. Related Work

Robotic systems have been introduced and used in biomechanics, neuroscience, and human movement science to study human postural balance. Those mechanical systems include one or two degree-of-freedom (DOF) moving plates (e.g., [18]), or multi-DOF robotic platforms (e.g., [19]) for testing dynamic posturography. Few robotic devices are designed to aim at studying or training the human's whole-body postural capability through unstable physical human-robot interactions. Our bikebot concept was inspired by the recent clinical studies in [20], [21] that report promising results of treating postural disorder and Parkinson's disease

This work was supported in part by the US National Science Foundation under awards CMMI-0954966 and CMMI-1334389.

Y. Zhang, P. Wang, and J. Yi are with the Department of Mechanical and Aerospace Engineering, Rutgers University, Piscataway, NJ 08854 USA (e-mail: yzzhang@eden.rutgers.edu, pengcheng.wang@rutgers.edu, jgyi@rutgers.edu).

D. Song is with the Department of Computer Science and Engineering, Texas A&M University, College Station, TX 77845 USA (e-mail: dzsong@cse.tamu.edu).

Preprint submitted to 2014 IEEE International Conference on Robotics and Automation. Received September 15, 2013.

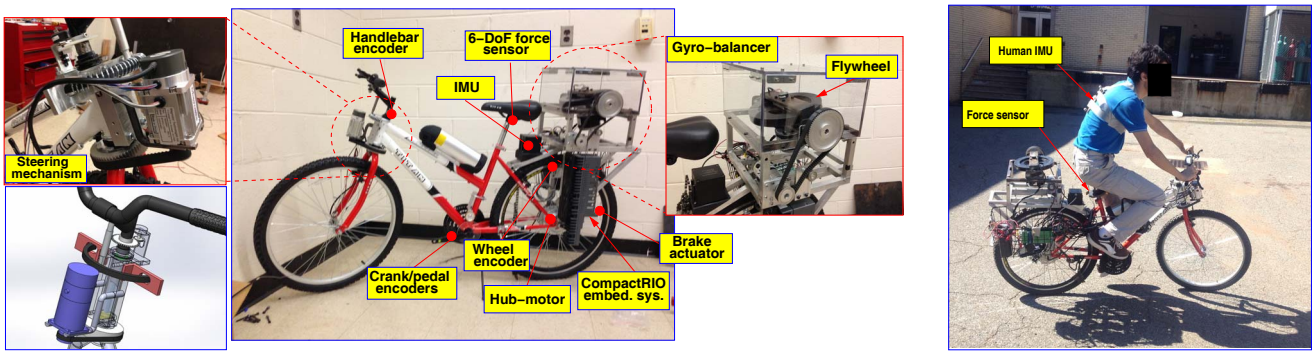

(a) (b)

Fig. 1. (a) The Rutgers bikebot for studying physical rider-robot interactions. The left sub-figure shows the modified steering mechanism that disengages the rider steering with the actual motorized steering fork. The right-figure shows the single gyro-balancer design. (b) Human riding experiment.

patients through bicycle riding. The bicycle-based rehabilitation device in [20] is a stationary platform and does not have the capability for dynamically sensing and perturbing human motor control skills. Our previous works [4], [6], [7] introduce a non-intrusive instrumented bicycle system and this type of instrumented bicycles however cannot actively perturb human motion and break the human neural control feedback loop. The bikebot instead extends the capability of the instrumented bicycle by a modified steering, driving and balancing mechanisms to augment the rider's dynamic postural balance capability.

This paper focuses on the dynamic modeling and balancing control of the bikebot. We extend the dynamic models in [4], [22] and include the gyro-balancer dynamics. Gyroscopic torques are used to help balancing the bicycle [11], [14], [17], [23] or the unicycle [24]–[26]. None of these developments include the balancing control at zero moving velocity, which is much more challenging than balancing a moving platform. In this paper, we demonstrate a gyro-balancer-based balancing control for the stationary bikebot. Moreover, all of the above-mentioned autonomous bicycles or unicycles are for riderless design while our bikebot design is a human-in-the-loop system. Indeed, the bikebot and its interactions with the rider provide a unique and new platform to study human dynamic postural balance motor skills.

Flywheel-based gyro-stabilizer is a compact actuator to provide a need of large torques for robotic applications [27], [28]. A single gimbal gyro-balancer such as the one in the bikebot design shown in Fig. 1(a) has a compact size and a simple mechanical design. However, a single gimbal gyro-balancer has some configuration limitations. For example, the pivoting angle or angular rate of the flywheel of the gyro-balancer is bounded in certain ranges due to the physical constraints. Also, the gyro-balancer not only produces balancing torque along the roll direction but also generates undesirable torques along the yaw direction. To overcome such limitations, it is desirable to operate the gyro-balancer's flywheel around the zero pivoting angle when the actuator is used to help balance the bikebot.

It is challenging to balance the bikebot at zero moving velocity. Inspired by the observation that an experienced human rider commonly oscillates his/her body or the steering mechanism for balancing a bicycle, we propose to design the balancing controller to stabilize the bikebot on an orbital trajectory around the vertical equilibrium position. When actuated only by the gyro-balancer, the riderless bikebot is an underactuated nonlinear system, similar to many other mechanical systems such as a pendubot or a Furuta pendulum. In [9], [10], [29], [30], an orbital stabilization design is presented for a class of underactuated nonlinear dynamic systems such as Furuta pendulum. In these designs, a virtual (displacement) constraint is first constructed between the actuated and the underactuated coordinates and then the control strategies are used to create oscillating orbits around the unstable equilibrium. Although the bikebot dynamics share similarities to those of an inverted-pendulum or a Furuta pendulum, some essential differences exist in the orbital stabilization design. We cannot directly apply the existing results to construct the virtual displacement constraints because the coupling effects between the actuated gyro-balancer and the underactuated bikebot are through balancing moments, rather than the coupled position constraints in an inverted-pendulum or a Furuta pendulum. We reduce the robot dynamics to obtain and design the constrained dynamic motion between the gyro-balancer and the bikebot. This constructive dynamic constraint-based control design can be generalized to other underactuated mechanical systems where forces or torques (rather than displacements) are coupled between the actuated and unactuated subsystems.

III. Bikebot Dynamic Model

A. Bikebot design

Fig. 1(a) shows the bikebot developed at Rutgers University. The mechanical structure of the bikebot is built on a mountain bicycle with significant modifications. Both the traction/braking and the steering functions are augmented to allow a human rider, an onboard computer, or both to balance the unstable platform. A hub motor and a DC motor are used for rear-wheel driving and front steering mechanism control, respectively. The steering mechanism is modified such that the steering handlebar and the steering fork are mechanical separated and independently controlled; see the left sub-figure in Fig. 1(a). The rider turns the handlebar and the human input steering angle is measured by the

Preprint submitted to 2014 IEEE International Conference on Robotics and Automation. Received September 15, 2013.

encoder. The onboard controller then turns the lower-steering mechanism at a commanded steering angle. Same design is applied to pedaling for control the bikebot moving velocity. A computer-controlled braking actuator is installed on the rear wheel to reduce the moving velocity. To perturb the rider's balancing torque, a single gimbal active controlled gyro-balancer is mounted on the back rack of the bikebot as shown in the right sub-figure in Fig. 1(a).

B. Bikebot model

The bikebot is considered as a three-part platform: a rear frame with the gyro-balancer structure and rear wheel, the front wheel and steering mechanism and the gyro-balance flywheel. Fig. 2 shows a schematic of the bikebot kinematics. We consider the following modeling assumptions: (1) the mass center W of the gyro-balancer is located at the rotating axis and therefore, its translational velocity is along the rear frame; and (2) the rear wheel contact point satisfies the nonholonomic constraint, i.e., zero lateral velocity.

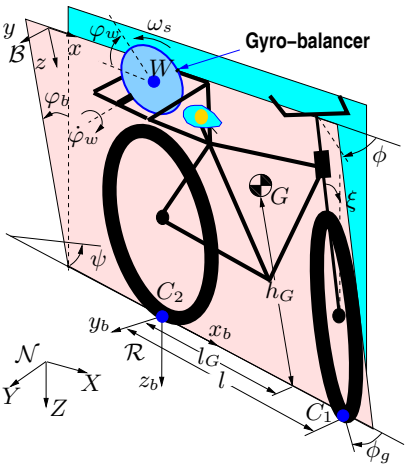

Fig. 2. Schematic of the gyro-balanced bikebot systems.

We denote C_1 and C_2 as the front and rear wheel contact points with the ground, respectively. As illustrated in Fig. 2, frame $\mathcal{B}(x, y, z)$ is setup on the rear frame with its origin at C_2, z-axis pointing downward, and x-axis pointing forward along C_2C_1. Two Euler angles, yaw angle ψ and roll angle φ_b, are used and the unit vector set of $\mathcal{B}$ is denoted as $(\boldsymbol{i}, \boldsymbol{j}, \boldsymbol{k})$.

From [22], the vertical position change Δh_G of the mass center G due to steering angle ϕ is captured as

$$\Delta h_G = l_G \Delta_s \tan\varphi_b \tan\phi, \tag{1}$$

where $\Delta_s = \frac{l_t \cos\xi}{l}\left[l_t\cos\xi - \frac{12R_t\xi}{\pi^2}\left(1-\frac{\sqrt{3}}{2}\right)\right]$, R_t is the radius of the front wheel, ξ is the caster angle, l and l_t are the wheelbase and trail distance, respectively. The translational velocity of C_2 and the angular velocity of the bikebot rear frame in $\mathcal{B}$ are respectively given as $\boldsymbol{v}_{C_2} = v_x\boldsymbol{i}$ and $\boldsymbol{\omega}_b = \dot{\varphi}_b\boldsymbol{i} + \dot{\psi}\,\mathrm{s}_{\varphi_b}\,\boldsymbol{j} + \dot{\psi}\,\mathrm{c}_{\varphi_b}\,\boldsymbol{k}$, where v_x is moving forward velocity and we use notations $\mathrm{c}_{\varphi_b} := \cos\varphi_b$ and $\mathrm{s}_{\varphi_b} := \sin\varphi_b$ for φ_b and other angles. The position of the mass center G in $\mathcal{B}$ is $\boldsymbol{\rho}_G = l_G\boldsymbol{i} - h_G\boldsymbol{k}$, where l_G and h_G are the horizontal and vertical distances from G to C_2, respectively. We thus obtain the velocity of G as

$$\boldsymbol{v}_G = (v_x - h_G\dot{\psi}\,\mathrm{s}_{\varphi_b})\boldsymbol{i} + (h_G\dot{\varphi}_b + l_G\dot{\psi}\,\mathrm{c}_{\varphi_b})\boldsymbol{j} - l_G\dot{\psi}\,\mathrm{s}_{\varphi_b}\,\boldsymbol{k}. \tag{2}$$

The flywheel's precession angular velocity is $\boldsymbol{\Omega}_w = \dot{\varphi}_b\boldsymbol{i} + (\dot{\psi}\,\mathrm{s}_{\varphi_b} + \dot{\varphi}_w)\boldsymbol{j} + \dot{\psi}\boldsymbol{k}$, where φ_w is the flywheel pivoting angle. The gyroscopic torque generated by the gyro-balancer along the x-axis direction is obtained

$$\begin{aligned}\tau_{wx} = {} & (I_{wz} - I_{wx})(\dot{\psi}^2\,\mathrm{c}_{\varphi_b}\,\mathrm{s}_{\varphi_b} + \dot{\psi}\dot{\varphi}_w\,\mathrm{c}_{\varphi_b}) + \\ & I_{wz}\omega_s\,\mathrm{c}_{\varphi_w}(\dot{\psi}\,\mathrm{s}_{\varphi_b} + \dot{\varphi}_w)\end{aligned} \tag{3}$$

where the flywheel inertia matrix is $\boldsymbol{I}_w = \mathrm{diag}\{I_{wx}, I_{wy}, I_{wz}\}$ with the assumption that the principle axes are along its body frame.

With the nonholonomic constraint at C_2 and the kinematic geometry [22], we obtain that $v_x = \frac{l}{\sigma}\dot{\psi}$ and $\sigma = \tan\phi_g$ with steering mechanism relationship $\tan\phi_g\,\mathrm{c}_\varphi = \tan\phi\,\mathrm{c}_\xi$. Using Lagrange's equations, we obtain the motion equations of the bikebot as

$$\begin{aligned}& (m_b h_G^2 + \mathrm{c}^2_{\varphi_w} I_{wx} + \mathrm{s}^2_{\varphi_w} I_{wz} + I_{bx})\ddot{\varphi}_b + m_b h_G \frac{\dot{\sigma}}{l} v_x\,\mathrm{c}_{\varphi_b} + \\ & 2(I_{wz} - I_{wx})\,\mathrm{s}_{\varphi_w}\,\mathrm{c}_{\varphi_w}\,\dot{\varphi}_w\dot{\varphi}_b + (\mathrm{s}^2_{\varphi_w} - \mathrm{c}^2_{\varphi_w})\frac{\sigma}{l} v_x\,\mathrm{c}_{\varphi_b}\,\dot{\varphi}_w I_{wx} \\ & - s_{\varphi_w}c_{\varphi_w}\left(\frac{\dot{\sigma}}{l}v_x + \frac{\sigma}{l}\dot{v}_x\right)c_{\varphi_b} I_{wx} (\mathrm{c}^2_{\varphi_w} - \mathrm{s}^2_{\varphi_w})\frac{\sigma}{l} v_x\,\mathrm{c}_{\varphi_b}\,\dot{\varphi}_w I_{wz} \\ & + \mathrm{s}_{\varphi_w}\,\mathrm{c}_{\varphi_w}\left(\frac{\dot{\sigma}}{l}v_x + \frac{\sigma}{l}\dot{v}_x\right)c_{\varphi_b} I_{wz} + \mathrm{c}_{\varphi_w}\,\dot{\varphi}_w\omega_s I_{wz} \\ & + m_b v_x^2 \frac{\sigma}{l}(1 - s_{\varphi_b}\frac{\sigma}{l}h_G)s_{\varphi_b}h_G + \frac{\sigma^2}{l^2}v_x^2 s_{\varphi_b}c_{\varphi_b}(I_{bz} - I_{bx}) \\ & + \frac{\sigma^2}{l^2}v_x^2(s_{\varphi_b}c_{\varphi_b}I_{wy} - s^2_{\varphi_w}s_{\varphi_b}c_{\varphi_b}I_{wx} - c^2_{\varphi_w}s_{\varphi_b}c_{\varphi_b}I_{fz}) \\ & + \frac{\sigma}{l}v_x c_{\varphi_b}\dot{\varphi}_w I_{wy} - c_{\varphi_w}\frac{\sigma}{l}v_x s_{\varphi_w}\omega_s I_{wz} + m_b g h_G\,\mathrm{s}_{\varphi_b} \\ & - m_b g l_G \Delta_s \tan\phi\sec^2\varphi_b = 0,\end{aligned} \tag{4}$$

$$\begin{aligned}& I_{wy}\ddot{\varphi}_w + \left(\frac{\dot{\sigma}}{l}v_x + \frac{\sigma}{l}\dot{v}_x\right)\mathrm{s}_{\varphi_b}\,I_{wy} + \frac{\sigma}{l}v_x\dot{\varphi}_b\,\mathrm{c}_{\varphi_b}\,I_{wy} + \\ & (I_{wz} - I_{wx})\dot{\varphi}_b^2\,\mathrm{c}_{\varphi_w}\,\mathrm{s}_{\varphi_w} + (\mathrm{s}^2_{\varphi_w} - \mathrm{c}^2_{\varphi_w})\frac{\sigma}{l}v_x\dot{\varphi}_b\,\mathrm{c}_{\varphi_b}(I_{wx} - I_{wz}) \\ & + \mathrm{s}_{\varphi_w}\,\mathrm{c}_{\varphi_w}\,\frac{\sigma^2}{l^2}v_x^2\,\mathrm{c}^2_{\varphi_b}(I_{wx} - I_{wz}) + \mathrm{s}_{\varphi_w}\,\frac{\sigma}{l}v_x\,\mathrm{c}_{\varphi_b}\,\omega_s I_{wz} \\ & - I_{wz}\dot{\varphi}_b\omega_s\,\mathrm{c}_{\varphi_w} = \tau_m,\end{aligned} \tag{5}$$

and

$$\begin{aligned}& m_b\dot{v}_x\left[\left(1 - h_G\frac{\sigma}{l}\mathrm{s}_{\varphi_b}\right)^2 + \frac{\sigma^2}{l^2}l_G^2\right] + \frac{\sigma^2}{l^2}\dot{v}_x\left(I_x\,\mathrm{s}^2_{\varphi_b} + I_z\,\mathrm{c}^2_{\varphi_b}\right) + \\ & 2m_b v_x\left[-\frac{h_G}{l}\left(1 - h_G\,\mathrm{s}_{\varphi_b}\,\frac{\sigma}{l}\right)(\dot{\sigma}\,\mathrm{s}_{\varphi_b} + \sigma\dot{\varphi}_b\,\mathrm{c}_{\varphi_b}) + \frac{\sigma\dot{\sigma}}{l^2}l_G^2\right] + \\ & 2\frac{\sigma\dot{\sigma}}{l^2}v_x\left(I_y\,\mathrm{s}^2_{\varphi_b} + I_z\,\mathrm{c}^2_{\varphi_b}\right) + 2\frac{\sigma^2}{l^2}v_x\dot{\varphi}_b(I_y - I_z)\,\mathrm{s}_{\varphi_b}\,\mathrm{c}_{\varphi_b} + \\ & m_b l_G h_G\frac{\dot{\sigma}}{l}\dot{\varphi}_b\,\mathrm{c}_{\varphi_b} + m_b l_G h_G\frac{\sigma}{l}\ddot{\varphi}_b\,\mathrm{c}_{\varphi_b} - m_b l_G h_G\frac{\sigma}{l}\dot{\varphi}_b^2\,\mathrm{s}_{\varphi_b} \\ & + \frac{\dot{\sigma}}{l}\dot{\varphi}_w\,\mathrm{s}_{\varphi_b}\,I_{wy} + \frac{\sigma}{l}\ddot{\varphi}_w\,\mathrm{s}_{\varphi_b}\,I_{wy} + \frac{\sigma}{l}\dot{\varphi}_b\dot{\varphi}_w\,\mathrm{c}_{\varphi_b}\,I_{wy} + \\ & \frac{\dot{\sigma}}{l}\omega_s\,\mathrm{c}_{\varphi_w}\,\mathrm{c}_{\varphi_b}\,I_{wz} - \frac{\sigma}{l}\dot{\varphi}_b\omega_s\,\mathrm{c}_{\varphi_w}\,\mathrm{s}_{\varphi_b}\,I_{wz} \\ & - \frac{\sigma}{l}\dot{\varphi}_w\omega_s\,\mathrm{c}_{\varphi_b}\,\mathrm{s}_{\varphi_w}\,I_{wz} = F_{rx},\end{aligned} \tag{6}$$

Preprint submitted to 2014 IEEE International Conference on Robotics and Automation. Received September 15, 2013.

where τ_m is the output torque of the gyro-balancer pivoting motor and F_{rx} is the traction/braking force of the bikebot rear wheel.

It is of a particular interest to consider a stationary bikebot. In this case, $v_x = 0$ and $\psi = 0$. The motion equations of the bikebot in (4)-(6) are reduced to

$$(m_b h_G^2 + I_x + I_{wxz}\,\mathrm{s}^2_{\varphi_w})\ddot{\varphi}_b + I_{wxz}\,\mathrm{s}_{2\varphi_w}\,\dot{\varphi}_w\dot{\varphi}_b - m_b g h_G\,\mathrm{s}_{\varphi_b} + I_{wz}\,\mathrm{c}_{\varphi_w}\,\dot{\varphi}_w\omega_s = m_b g l_G \Delta_s \sec^2\varphi_b \tan\phi, \quad (7)$$

$$I_{wy}\ddot{\varphi}_w + I_{wxz}\dot{\varphi}_b^2\,\mathrm{c}_{\varphi_w}\,\mathrm{s}_{\varphi_w} - I_{wz}\dot{\varphi}_b\omega_s\,\mathrm{c}_{\varphi_w} = \tau_m, \quad (8)$$

where $I_{wxz} = I_{wz} - I_{wx}$.

In the rest of the paper, we focus on stationary bikebot balancing control and analysis and also on the experimental demonstration of the perturbed rider-bikebot interactions.

IV. Stationary Balancing Control and Analysis

A. Stationary bikebot dynamics

We define the state variable $\boldsymbol{x} = [x_1 \;\; x_2 \;\; x_3]^T = [\varphi_b \;\; \dot{\varphi}_b \;\; \sin\varphi_w]^T$. For presentation convenience, we also define $\boldsymbol{x}_b = [x_1 \;\; x_2]^T$. Since the pivoting motor is controlled through the lower-level embedded control for a given velocity, we consider a velocity control input for pivoting angle x_3. With the defined state variable, we re-write the dynamics (7) along with the pivoting angular velocity control as

$$\dot{x}_1 = x_2 \quad (9a)$$

$$\dot{x}_2 = f(\boldsymbol{x}) + g_1(\boldsymbol{x})u_1 + g_2(\boldsymbol{x})u_2 \quad (9b)$$

$$\dot{x}_3 = u_1, \quad (9c)$$

where $u_1 = \mathrm{c}_{\varphi_w}\,\dot{\varphi}_w$ is the controlled pivoting velocity, $u_2 = \tan\phi$ is the controlled steering input,

$$f(\boldsymbol{x}) = \frac{m_b g h_G\,\mathrm{s}_{x_1}}{I_s(\boldsymbol{x})},\; g_1(\boldsymbol{x}) = -\frac{I_{wxz}x_2\,\mathrm{s}_{2x_3} + I_{wz}\omega_s}{I_s(\boldsymbol{x})},\; g_2(\boldsymbol{x}) = \frac{m_b g l_G \Delta_s \sec^2 x_1}{I_s(\boldsymbol{x})}, \quad (10)$$

and $I_s(\boldsymbol{x}) = m_b h_G^2 + I_x + I_{wxz}\,\mathrm{s}^2_{x_3}$. Due to the physical constraints, the pivoting angle and angular rate are within certain ranges, namely,

$$|x_3| = |\,\mathrm{s}_{\varphi_w}\,| \le \mathrm{s}_{\varphi_w^{\max}} < 1,\; |u_1| = |\,\mathrm{c}_{\varphi_w}\,\dot{\varphi}_w| \le \omega_w^{\max}, \quad (11)$$

where $\varphi_w^{\max}$ and $\omega_w^{\max}$ are the maximum flywheel pivoting angle and angular velocity, respectively.

Without steering control (i.e., $u_2 = 0$), the equilibrium of the dynamics (9) is $x_{1e} = x_{2e} = 0$ under $u_{1e} = \dot{\varphi}_{we} = 0$. It is interesting to notice that the flywheel pivoting angle can be any values within $\varphi_w^{\max}$ while the bikebot is balanced.

We consider how to compute the gyro-balancer flywheel's pivoting angle $x_3(t)$ for a given profile for bikebot roll angle $x_1(t)$. Indeed, (7) can be re-written as

$$\frac{d}{dt}\Big[(m_b h_G^2 + I_x)x_2 + I_{wxz}\dot{\varphi}_b x_3^2 + I_{wz}\omega_s x_3\Big] = -\frac{\partial}{\partial\varphi_b}\Big(m_b g h_G\,\mathrm{c}_{x_1}\Big) \quad (12)$$

and thus, the bikebot satisfies the Hamiltonian dynamics with angular momentum along the x-axis direction

$$p_x(t) = (m_b h_G^2 + I_x)x_2(t) + I_{wxz}x_2(t)x_3^2(t) + I_{wz}\omega_s x_3(t). \quad (13)$$

By integrating (12), it is then straightforward to obtain

$$p_x(t) - p_x(0) = \int_0^t m_b g h_G\,\mathrm{s}_{x_1(\tau)}\,d\tau. \quad (14)$$

From (14), we have the following property with a proof given in Appendix I.

Property 1: For a given periodic profile $x_1(t)$ with period T, the profile for the pivoting angle is also periodic with period T.

With the results in Property 1, we design an orbital stabilization control to synchronize the periodic motion between the flywheel pivoting motion (x_3) and the bikebot roll motion (x_1).

B. Balancing controller

We consider the balancing controller design by using the gyro-balancer and the steering mechanism separately.

1) Gyro-balancer-based balancing control: To further simplify the controller design, from (10) and the fact that the flywheel spinning speed $\omega_s \gg |x_2|$, it is noted that $I_{wz}\omega_2\,\mathrm{c}_{x_3} \gg |I_{wxz}x_2\,\mathrm{s}_{2x_3}|$. Moreover, $m_b h_G^2 \gg I_x \gg I_{wxz}$ and therefore, (9b) is approximated as

$$\dot{x}_2 - \frac{g}{h_G}\,\mathrm{s}_{x_1} + \frac{I_{wz}\omega_s}{m_b h_G^2}u_1 = 0. \quad (15)$$

Clearly, for simplified dynamics (15), state variable $\boldsymbol{x} \in \mathcal{D} := \mathbb{S}\times\mathbb{R}\times(-1,1)$.

We consider regulating the bikebot roll motion on an orbital trajectory in $\mathcal{D}$. An oscillation orbital trajectory $\mathcal{O}_b$ is given by the following pendulum dynamics.

$$\mathcal{O}_b:\; \dot{x}_2 + \frac{b}{h_G}\,\mathrm{s}_{x_1} = 0, \quad (16)$$

where design parameter $b > 0$ is a gravitationally equivalent constant. Plugging (16) into dynamics (15) to eliminate term s_{x_1}, we obtain

$$\dot{x}_3 = -\frac{(b+g)m_b h_G^2}{I_{wz}b\omega_s}\dot{x}_2 = -L\dot{x}_2, \quad (17)$$

where constant $L = \frac{(g+b)m_b h_G^2}{I_{wz}b\omega_s}$. Therefore, by integrating (17), the corresponding orbital trajectory $\mathcal{O}_w$ for x_3 is obtained as

$$\mathcal{O}_w:\; x_3 = -Lx_2. \quad (18)$$

Remark 1: The form of (18) is seemingly similar to those of virtual holonomic constraints in orbital stabilization of underactuated mechanical systems in [9], [10]. However, the relationships (18) are not the same as the virtual constraints in [9], [10] because (18) is obtained through the system dynamics (15) rather than by design. Moreover, (18) represents the torque balance relationship between the controlled flywheel pivoting and the underactuated bikebot roll motion, while the virtual holonomic constraints in [9], [10] capture the displacement relationships among the coordinates.

Preprint submitted to 2014 IEEE International Conference on Robotics and Automation. Received September 15, 2013.

Once the bikebot roll motion follows orbit $\mathcal{O}_b$, the total energy $E(\boldsymbol{x}_b)$ is defined as:

$$E(\boldsymbol{x}_b) = \frac{1}{2} m_b h_G^2 x_2^2 + m_b h_G b \left(1 - \mathrm{c}_{x_1}\right).$$

When target orbit $\mathcal{O}_b$ reaches the maximum angle x_1^d with $x_2 = 0$, the total energy is $E_d = m_b h_G b(1 - \mathrm{c}_{x_1^d})$. We define the energy difference $\Delta E = E(\boldsymbol{x}_b) - E_d$ and consider the Lyapunov candidate function $V(\boldsymbol{x})$ as

$$V_1(\boldsymbol{x}) = \frac{1}{2}\Delta E^2 + \frac{1}{2} k_1 \left(x_3 + L x_2\right)^2,$$

where $k_1 > 0$ is a constant. Obviously, $V_1(\boldsymbol{x}) \geq 0$ and

$$\dot{V}_1(\boldsymbol{x}) = \Delta E(m_b h_G^2 x_2 \dot{x}_2 + m_b h_G b\, \mathrm{s}_{x_1} x_2) + k_1(x_3 + L x_2)(\dot{x}_3 + L\dot{x}_2).$$

Using (9) and (15) and letting

$$u_1 = \frac{Lb}{h_G}\left(\mathrm{s}_{x_1} + v_1\right) = u_{1s} + \frac{Lb}{h_G} v_1, \tag{19}$$

where $u_{1s} = \frac{Lb}{h_G}\mathrm{s}_{x_1}$ and v_1 is an auxiliary control input, $\dot{V}_1(\boldsymbol{x})$ is then reduced to

$$\dot{V}_1(\boldsymbol{x}) = -m_b h_G (g + b)\left[\Delta E x_2 + \alpha k_1 \left(x_3 + L x_2\right)\right] v_1,$$

where $\alpha = \frac{g}{bI_{wz}\omega_s} > 0$ is a constant.

The control input v is further designed as

$$v_1 = k_2 \left[\Delta E x_2 + \alpha k_1 \left(x_3 + L x_2\right)\right] \tag{20}$$

with a positive constant parameter $k_2 > 0$ and then we obtain

$$\dot{V}_1(\boldsymbol{x}) = -m_b h_G (g + b) k_2 \left[\Delta E x_2 + \alpha k_1 \left(x_3 + L x_2\right)\right]^2 \leq 0.$$

By LaSalle theory [31], the system states asymptotically converge to the invariant set $\mathcal{S}(\boldsymbol{x})$

$$\mathcal{S}(\boldsymbol{x}) = \left\{\boldsymbol{x} \in \mathcal{D} \,|\, \Delta E x_2 + \alpha k_1 \left(x_3 + L x_2\right) = 0\right\}. \tag{21}$$

In $\mathcal{S}(\boldsymbol{x})$, $v = 0$, $u_1 = u_{1s}$ and the trajectories of the closed-loop dynamics are on orbits $\mathcal{O}_b$ and $\mathcal{O}_w$. It is straightforward to obtain that origin $\boldsymbol{x}_e = \mathbf{0} \in \mathcal{S}(\boldsymbol{x})$.

If the states are not at origin in $\mathcal{S}(\boldsymbol{x})$, i.e., $\boldsymbol{x} \in \mathcal{S}(\boldsymbol{x}) \setminus \{\mathbf{0}\}$, ΔE is a constant with the periodical varying x_2 and from (17), we obtain $x_3 + L x_2 = C$ (constant). Given the invariant set property in (21), this implies that in $\mathcal{S}(\boldsymbol{x}) \setminus \{\mathbf{0}\}$, $E = E_d$ (i.e., $\Delta E = 0$) and $x_3 + L x_2 = 0$. Thus, a subset of the invariant orbit $\mathcal{O}_w$ given by

$$\mathcal{O}_w^*(\boldsymbol{x}) = \left\{\boldsymbol{x} \in \mathcal{D} \,|\, \Delta E = 0,\, x_3 + L x_2 = 0\right\}$$

also lies in $\mathcal{S}(\boldsymbol{x})$, namely, $\mathcal{O}_w^* = \mathcal{S}(\boldsymbol{x}) \setminus \{\mathbf{0}\}$. By LaSalle principle, under the control (19), the state variables converge to the target orbits $\mathcal{O}_b$ and $\mathcal{O}_w^*$ asymptotically for an initial state $\boldsymbol{x}(0)$ in the domain of attraction $\mathcal{D}_1 \subset \mathcal{D}$. We will give an estimate of $\mathcal{D}_1$ later in this section.

2) Steering-based balancing control: In this section, we design a balancing control strategy only using steering mechanism, i.e., $u_1 = 0$ in (9). Similar to the previous case, we use an energy shaping approach to design the controller as follows. Same as (15), we re-write (9b) as

$$\dot{x}_2 - \frac{g}{h_G}\mathrm{s}_{x_1} + \frac{g l_G \Delta_s \sec_{x_1}^2}{h_G^2} u_2 = 0. \tag{22}$$

We still consider the targeted orbit $\mathcal{O}_b$ in (16) for the desired bikebot motion. Following the same definition of $E(\boldsymbol{x}_b)$ and ΔE in the previous section, we consider the Lyapunov function candidate $V_2 = \frac{1}{2}\Delta E^2$. The steering control is obtained as

$$u_2 = u_{2s} + \frac{\mathrm{c}_{x_1}^2}{m_b g l_G \Delta_s} v_2, \tag{23}$$

where $u_{2s} = -\frac{(g+b)h_G\, \mathrm{c}_{x_1}^2}{g l_G \Delta_s}\mathrm{s}_{x_1}$ and the auxiliary control input v_2 is designed as

$$v_2 = -k_3 x_2 \Delta E$$

in which $k_3 > 0$ is a constant. It is straightforward to obtain that under control (23), $\dot{V}_2 = -k_3 x_2^2 \Delta E^2 \leq 0$. Following the same discussion in the previous section, under control (23) the bikebot roll motion will follow orbit $\mathcal{O}_b$ if the initial condition is in the domain of attraction $\mathcal{D}_2$.

We give an estimate of the domain of attraction $\mathcal{D}_1$ under the gyro-balancer control (19) and due to the page limit, we omit the estimate of $\mathcal{D}_2$ under steering control (23).

From the previous analysis, under control (19), $\boldsymbol{x} \in \mathcal{S}(\boldsymbol{x})$, $\dot{V}_1(\boldsymbol{x}) = 0$, and $\boldsymbol{x} = \mathbf{0}$, $V_1(\mathbf{0}) = \frac{1}{2}E_d^2$; $\boldsymbol{x} \in \mathcal{O}_w^*(\boldsymbol{x})$, $V_1(\boldsymbol{x}) = 0$. Therefore, a conservative estimate of $\mathcal{D}_1$ is

$$\mathcal{D}_1(\boldsymbol{x}) = \left\{\boldsymbol{x} \in \mathcal{D} \,|\, V_1(\boldsymbol{x}) \leq \frac{1}{2}E_d^2\right\}. \tag{24}$$

The calculation and example plots of $\mathcal{D}_1$ will be presented in the next section.

V. Experiments

A. Bikebot and experimental setup

Fig. 1(a) shows the bikebot prototype. The physical parameter values of the bikebot are obtained experimentally and listed in Table I. A force/torque sensor (from JR3 Inc.) is installed along the seat supporting rod to measure the 3-axis hip-seat forces and torques; see Fig. 1(a). Three load cells are installed inside the custom-built bicycle seat to measure the sitting force distribution. An optical encoder is used to measure the bicycle speed. One IMU unit (model 800 from Motion Sense Inc.) is mounted to the bicycle frame. The IMU provides the bicycle attitude estimation for real-time balancing control. For human riding experiment, a second IMU is attached at the back of the rider to measure the upper-body pose [7]; see Fig. 1(b). Each IMU consists of a tri-axial gyroscope and a tri-axial accelerometer. The embedded system (NI cRIO 9082 real-time system) samples and stores all sensor measurements at the frequency of 100 Hz and also controls the motors at the same frequency.

For indoor self-balance experiments, a vision-based motion capture system (from Vicon Inc.) is used to provide the

Preprint submitted to 2014 IEEE International Conference on Robotics and Automation. Received September 15, 2013.

TABLE I

BIKEBOT PHYSICAL PARAMETERS

m_b (kg)	I_{bx} (kgm^2)	I_{wx} (kgm^2)	I_{wz} (kgm^2)	h_G (m)	l_G (m)	l (m)	l_t (m)	ξ (deg)	R_t (m)	ω_s (rpm)
51	2.5	0.028	0.036	0.64	0.27	1.1	0.06	20	0.33	1080

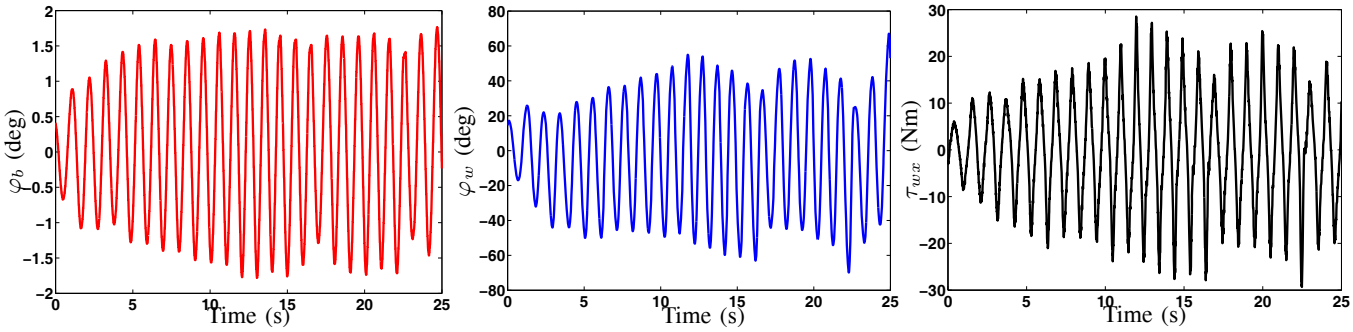

(a) (b) (c)

Fig. 3. Bikebot self-balancing at zero velocity using the gyro-balancer control. (a) Bikebot roll angle φ_b. (b) Gyro-balancer flywheel pivoting angle φ_w. (c) The controlled turning torque τ_{wx}.

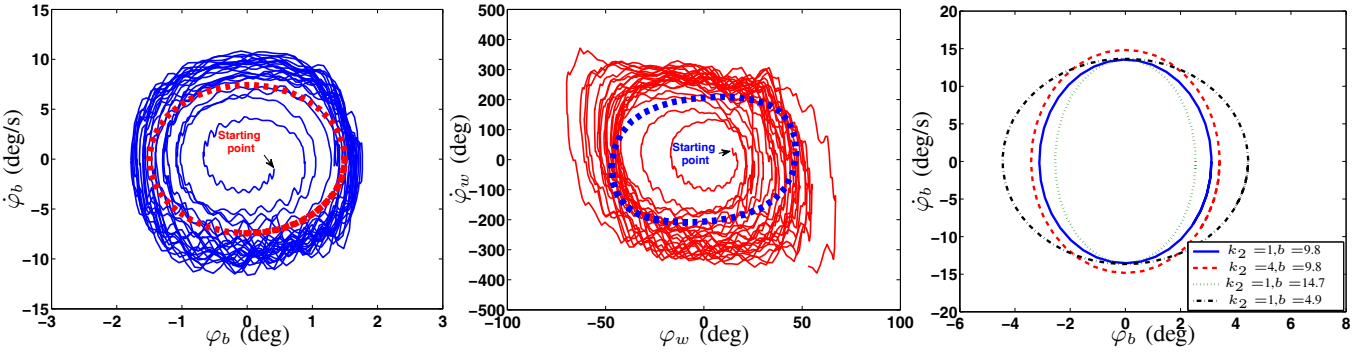

(a) (b) (c)

Fig. 4. Phase portraits of the stationary bikebot self-balancing control. (a) Bikebot roll motion $\dot{\varphi}_b$ vs. φ_b. The thick dashed line indicates the orbit $\mathcal{O}_b$. (b) Gyro-balancer flywheel motion $\dot{\varphi}_w$ vs. φ_w. The thick dashed line indicates the orbit $\mathcal{O}_w$. (c) The estimated domain of attraction $\mathcal{D}_1$ projected on plane φ_b-$\dot{\varphi}_b$.

ground truth for the bicycle roll angle. The motion capturing systems are synchronized with the onboard sensors through the wireless network connections. For outdoor experiments, the bicycle attitude angles are obtained by a high accuracy bicycle IMU.

B. Autonomous stationary balancing experiments

We demonstrate the gyro-balancer-based control of the stationary bikebot in experiments. Due to the page limit, we will not present the balancing experiments under the steering-based control. The gyro-balancer-based balancing controller (19) was implemented with parameter $b = 1$ and $k_2 = 1$ and the bikebot was successfully balanced. Fig. 3 shows the experimental results. The bikebot roll angle is shown in Fig. 3(a), the gyro-balancer flywheel pivoting angle is shown in Fig. 3(b) and the generated gyroscopic balancing torque is shown in Fig. 3(c). Clearly, the trajectories of the bikebot roll angle and the pivoting angle converge to the orbits and are finally synchronized in a periodic motion. It is also clear that under the gyro-balancer control constraint (11), the bikebot can be balanced within a small range (i.e., 2-3 degs.) around the vertical position.

The synchronized motion between the bikebot roll and flywheel pivoting motions can be further observed from the phase portraits shown in Fig. 4. Fig. 4(a) shows the phase portrait of the bikebot roll motion, Fig. 4(b) of the flywheel pivoting motion and Fig. 4(c) is the domain of attraction estimation (24) projected on the roll motion plane. The results shown in these plots confirm the design of the orbital stabilization design and also demonstrate that the controlled bikebot motion is within the DOA estimate.

C. Human-bikebot interaction experiments

To demonstrate the feasibility of the use of the bikebot to perturb the human motor control and coordination, we also conduct a set of human riding experiments. A young male subject with experienced bicycle riding skills was recruited to ride the bikebot in outdoor environment; see Fig. 1(b). The subject was asked to ride the bikebot same as his regular bicycle riding style. Both a straight-line riding (for a distance of 50 m) and a circular riding (about a radius of 3 m) were conducted in experiments. After the subject got used to ride the bikebot comfortably, we turned on the gyro-balancer to

Preprint submitted to 2014 IEEE International Conference on Robotics and Automation. Received September 15, 2013.

perturb the riding and measured the rider's responses to the generated torque disturbances.

We first perturbed the riding by a single torque disturbance suddenly applied without notifying the rider. Fig. 5 shows the steering angle responses and the perturbed torques for both the straight-line and circular bikebot riding experiments. It is clearly shown in these plots that under a perturbation, the rider uses the steering as a motor control strategy to keep balancing the unstable platform. The responses also confirm the "counter-steering" strategy (turning the steering toward the same direction as falling trend), a bicycle-riding motor skill that is obtained through training.

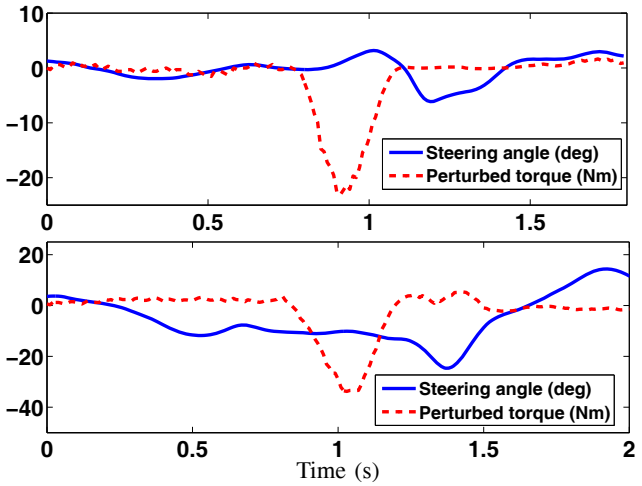

Fig. 5. Steering angle and a single perturbed torque disturbance. Top: along a straight-line trajectory. Bottom: along a circular trajectory.

To further demonstrate that riders use steering, rather than other motor strategies such as upper body motions, as an effective strategy in the straight-line and circular riding, we conduct riding experiments under randomly generated torques. We compare the riding responses in these perturbed experiments with profiles obtained from normally riding experiments without any disturbances. Fig. 6 shows the comparison results of the rider-bikebot interactions under a normal and a perturbed experiment. Fig. 6(a)-6(c) shows the rider's steering angle responses, bikebot roll angle, and the rider applied torque in the roll angle direction for straight-line riding and Fig. 6(d)-6(f) shows the profiles of the same variables for circular riding experiments. The rider responded to the random perturbation by actively turning the handlebar and using steering to balance the platform in experiments. This is clearly observed by the comparison with normal riding behavior shown in Fig. 6(a) and 6(d). On the other hand, neither of the comparisons of the bikebot roll angle profiles shown in Fig. 6(b) and 6(e) nor rider applied torques shown in Fig. 6(b) and 6(e) does clearly demonstrate significant difference. These results and observations confirm that the bikebot platform can be used to study dynamic postural human motor skills.

VI. Conclusion and Future Work

We reported the development of the bikebot for studying human dynamic postural balance motor control. The bikebot was modified from a bicycle platform to argument the rider's capability with actuated steering, driving and balancing capabilities. This paper presented a dynamic model of the bikebot with a gyro-balancer actuator. A self-balancing control was designed to stabilize the riderless, underactuated stationary bikebot on motion orbits. The stability and the stable regions were also obtained through analysis. We demonstrated the controller design and analysis through experiments. Riding experiments were also presented to demonstrate the feasibility to use the bikebot platform to study and tune human dynamic postural control.

We currently work on using the bikebot to model human dynamic postural balance and motor control skills. Development of an integrated steering/gyro-balancer control and its interactions with human motor control is another ongoing task.

References

[1] D. J. Reinkensmeyer and J. L. Patton, "Can robots help the learning of skilled actions?" *Exerc. Sport Sci. Rev.*, vol. 37, no. 1, pp. 43–51, 2008.

[2] C. Yang, G. Ganesh, S. Haddadin, S. Parusel, A. Albu-Schäeffer, and E. Burdet, "Human-like adaptation of force and impedance in stable and unstable interactions," *IEEE Trans. Robotics*, vol. 27, no. 5, pp. 918–930, 2011.

[3] S. Ikemoto, H. B. Amor, T. Minato, B. Jung, and H. Ishiguro, "Physical human-robot ineraction: Mutual learning and adaptation," *IEEE Robot. Automat. Mag.*, vol. 19, no. 4, pp. 24–35, 2012.

[4] J. Yi, D. Soudbakhsh, Y. Zhang, and Y. Zhang, "Why some Parkinson's disease patients cannot stand or walk but can ride a bicycle – A control system-based analysis," in *Proc. ASME Dyn. Syst. Control Conf.*, Ft. Lauderdale, FL, 2012, Paper # DSCC2012-8735.

[5] Y. Zhang and J. Yi, "Dynamic modeling and balance control of human/bicycle systems," in *Proc. IEEE/ASME Int. Conf. Adv. Intell. Mechatronics*, Montreal, Canada, 2010, pp. 1385–1390.

[6] K. Chen, Y. Zhang, and J. Yi, "Modeling rider/bicycle interactions with learned dynamics on constrained embedding manifolds," in *Proc. IEEE/ASME Int. Conf. Adv. Intell. Mechatronics*, Wollongong, Australia, 2013, pp. 442–447.

[7] Y. Zhang, K. Chen, and J. Yi, "Rider trunk and bicycle pose estimation with fusion of force/inertial sensors," *IEEE Trans. Biomed. Eng.*, vol. 60, no. 9, pp. 2541–2551, 2013.

[8] H. van der Kooij, R. Jocob, B. Koopman, and H. Grootenboer, "A multisensory integration model of human stance control," *Biol. Cybern.*, vol. 80, pp. 299–308, 1999.

[9] A. S. Shiriaev, J. W. Perram, and C. Canudas-de-Wit, "Constructive tool for orbital stabilization of underactuated nonlinear systems: Virtual constraints approach," *IEEE Trans. Automat. Contr.*, vol. 50, no. 8, pp. 1164–1176, 2005.

[10] A. S. Shiriaev, L. B. Freidovich, A. Robertsson, R. Johansson, and A. Sandberg, "Virtual-holonomic-constraints-based design of stable oscillations of Furuta pendulum: Theory and experiments," *IEEE Trans. Robotics*, vol. 23, no. 4, pp. 827–832, 2007.

[11] A. Beznos, A. Formal'sky, E. Gurfinkel, D. Jicharev, A. Lensky, K. Savitsky, and L. Tchesalin, "Control of autonomous motion of two-wheel bicycle with gyroscopic stabilisation," in *Proc. IEEE Int. Conf. Robot. Autom.*, Leuven, Belgium, 1998, pp. 2670–2675.

[12] S. Lee and W. Ham, "Self-stabilzing strategy in tracking control of unmanned electric bicycle with mass balance," in *Proc. IEEE/RSJ Int. Conf. Intell. Robot. Syst.*, Lausanne, Switzerland, 2002, pp. 2200–2205.

[13] J. Yi, D. Song, A. Levandowski, and S. Jayasuriya, "Trajectory tracking and balance stabilization control of autonomous motorcycles," in *Proc. IEEE Int. Conf. Robot. Autom.*, Orlando, FL, 2006, pp. 2583–2589.

[14] B. T. Thanh and M. Parnichkun, "Balancing control of bicyrobo by particle swarm optimization-based structure-specified mixed H_2/H_∞ control," *Int. J. Adv. Robotic Syst.*, vol. 5, no. 4, pp. 395 – 402, 2008.

[15] V. Cerone, D. Andreo, M. Larsson, and D. Regruto, "Stabilization of a riderless bicycle: A linear-parameter-varying approach," *IEEE Control Syst. Mag.*, vol. 30, no. 5, pp. 23–32, 2010.

Preprint submitted to 2014 IEEE International Conference on Robotics and Automation. Received September 15, 2013.

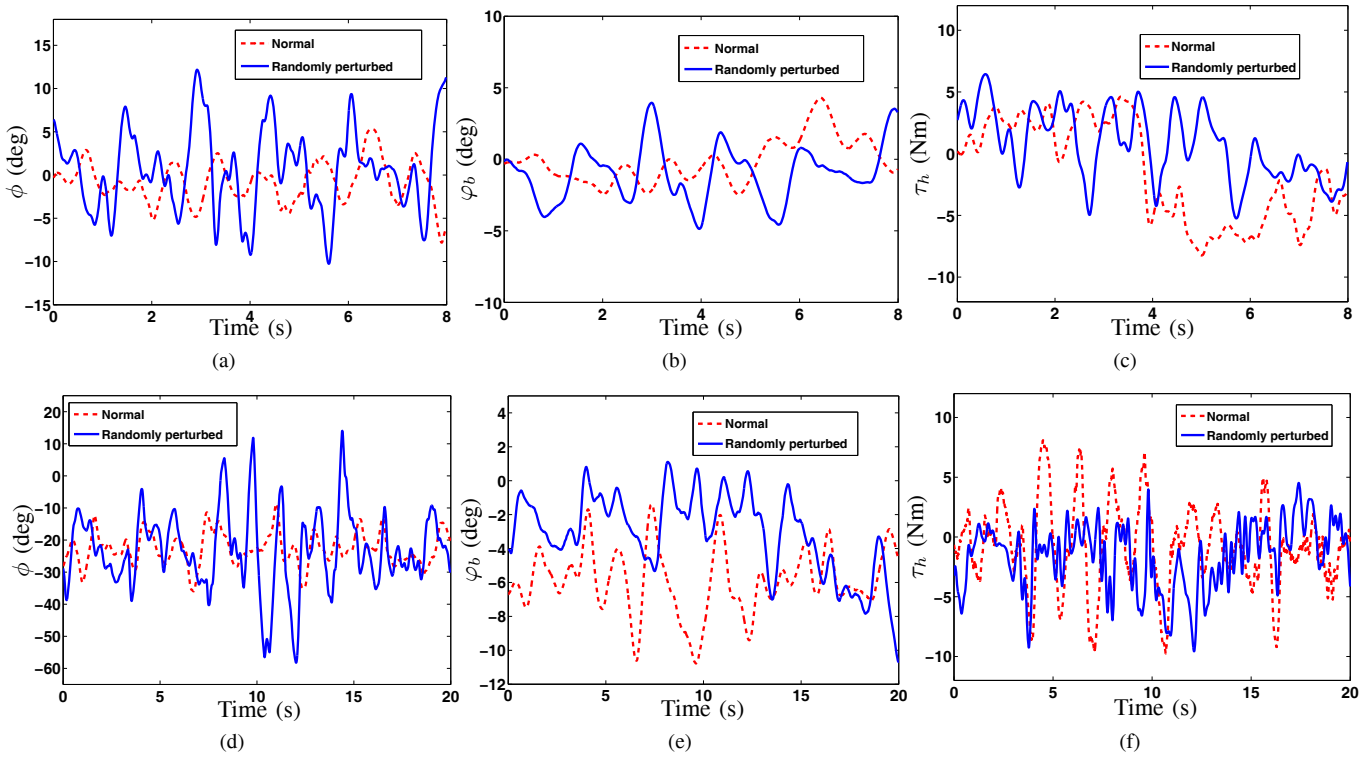

Fig. 6. Rider-bikebot responses under typical riding and randomly perturbation by the gyro-balancer for the straight-line (top row) and circular (bottom row) trajectories. (a) Steering angle ϕ for straight-line. (b) Bikebot roll angle φ_b for straight-line. (c) Rider applied torque τ_h on the seat for straight-line. (d) Steering angle ϕ for straight-line. (e) Bikebot roll angle φ_b for straight-line. (f) Rider applied torque τ_h on the seat for straight-line.

[16] Y. Tanaka and T. Murakami, "A study on straight-line tracking and posture control in electric bicycle," *IEEE Trans. Ind. Electron.*, vol. 56, no. 1, pp. 159–168, 2009.

[17] L. Keo and M. Yamakita, "Control of an autonomous electric bicycle with both steering and balancer controls," *Adv. Robot.*, vol. 25, no. 1-2, pp. 1–22, 2011.

[18] A. D. Goodworth and R. J. Peterka, "Influence of bilateral vestibular loss on spinal stabilization in humans," *J. Neurophysiol.*, vol. 103, pp. 1978–1987, 2010.

[19] F. Patané and P. Cappa, "A 3-DOF parallel robot with spherical motion for the rehabilitation and evaluation of balance performance," *IEEE Trans. Neural Syst. Rehab. Eng.*, vol. 19, no. 2, pp. 157–166, 2011.

[20] C.-G. Song, J.-Y. Kim, and N.-G. Kim, "A new postural balance control system for rehabilitation training based on virtual cycling," *IEEE Trans. Inform. Technol. Biomed.*, vol. 8, no. 2, pp. 200–207, 2004.

[21] M. B. Aerts, W. F. Abdo, and B. R. Bloem, "The "bicycle sign" for atypical parkinsonism," *Lancet*, vol. 377, pp. 125–126, 2011.

[22] Y. Zhang, J. Li, J. Yi, and D. Song, "Balance control and analysis of stationary riderless motorcycles," in *Proc. IEEE Int. Conf. Robot. Autom.*, Shanghai, China, 2011, pp. 3018–3023.

[23] S. C. Spry and A. R. Girard, "Gyroscopic stabilization of unstable vehicles: Configurations, dynamics, and control," *Veh. Syst. Dyn.*, vol. 46, no. Supp., pp. 247–260, 2008.

[24] Z. Sheng and K. Yamafuji, "Postural stability of a human riding a unicycle and its emulation by a robot," *IEEE Trans. Robot. Automat.*, vol. 13, no. 5, pp. 709–720, 1997.

[25] Y. Xu and S.K.-W. Au, "Stabilzation and path following of a single wheel robot," *IEEE/ASME Trans. Mechatronics*, vol. 9, no. 2, pp. 407–419, 2004.

[26] J. Lee, S. Han, and J. Lee, "A balancing control strategy for a one-wheel pendulum robot based on dynamic model decomposition: Simulations and experiments," *IEEE/ASME Trans. Mechatronics*, vol. 16, no. 4, pp. 763–768, 2011.

[27] B. Thornton, T. Ura, Y. Nose, and S. Turnock, "Zero-G class underwater robots: Unrestricted attitude control using control moments gyros," *IEEE J. Oceanic Eng.*, vol. 32, no. 3, pp. 565–583, 2007.

[28] N. C. Townsend and R. A. Shenoi, "Gyrostabilizer vehicular technology," *Appl. Mech. Rev.*, vol. 64, no. 1, pp. 010 801–1 – 010 801–14, 2011.

[29] M.-S. Park and D. Chwa, "Orbital stabilization of inverted-pendulum systems via coupled sliding-mode control method," *IEEE Trans. Ind. Electron.*, vol. 56, no. 9, pp. 3556–3570, 2009.

[30] L. B. Freidovich, A. S. Shiriaev, F. Gordillo, F. Gómez-Estern, and J. Aracil, "Partial-energy-shaping control for orbital stabilization of high-frequency oscillations of the Furuta pendulum," *IEEE Trans. Contr. Syst. Technol.*, vol. 17, no. 4, pp. 853–858, 2009.

[31] H. K. Khalil, *Nonlinear Systems*, 3rd ed. Upper Saddle River, NJ: Prentice Hall, 2002.

APPENDIX I
PROOF OF PROPERTY 1

For a periodic profile $x_1(t+T) = x_1(t)$ for any t, $x_2(t) = \dot{x}_1(t)$ is also periodic with period T, i.e., $x_2(t+T) = x_2(t)$. From (14), we obtain

$$p_x(t+T) - p_x(0) = \int_0^{t+T} m_b g h_G \, \mathrm{s}_{x_1(\tau)} \, d\tau.$$

Taking the difference of the above equation with (14), we obtain

$$p_x(t+T) - p_x(t) = \int_0^{T} m_b g h_G \, \mathrm{s}_{x_1(\tau)} \, d\tau. \qquad (25)$$

Using the fact that both $x_1(t)$ and $x_2(t)$ are periodic functions with period T and $\int_0^T \mathrm{s}_{x_1(\tau)} \, d\tau = 0$, using (13), (25) reduces to

$$[x_3(t+T) - x_3(t)] \, [I_{wz}\omega_s + I_{wxz}(x_3(t+T) + x_3(t))] = 0.$$

Thus, $x_3(t+T) = x_3(t)$ and the flywheel's pivoting angle is periodic with period T. This completes the proof.

Preprint submitted to 2014 IEEE International Conference on Robotics and Automation. Received September 15, 2013.